CHARACTERIZATION OF URBAN SAR PERMANENT SCATTERERS

Daniele Perissin[(1)], Claudio Prati[(1)]

[(1)] Politecnico di Milano, Piazza L. da Vinci 32, 20133 Milano, Italy, Email: perissin@elet.polimi.it

KEY WORDS: Permanent Scatterers, SAR Interferometry, SAR Polarimetry.

ABSTRACT:

The recently developed Permanent Scatterers (PS) technique is a processing tool in the field of space-borne SAR interferometry to detect terrain deformations with millimetre accuracy. Such accuracy is achieved in correspondence of privileged targets, the so-called Permanent Scatterers. Even if the PS technique is an operational tool since 2001, the physical nature of the PS's is still a subject of investigation. A good knowledge of the PS nature is an essential step to improve the interpretation of the measured ground deformation and to get a more precise topographic reconstruction. In this work we present the last results of the PS characterization obtained by using 120 ERS and ENVISAT repeated acquisitions on the urban area of Milano (Italy).

RIASSUNTO:

La tecnica dei diffusori permanenti (Permanent Scatterers, PS) è un'applicazione di punta nel contesto dell'interferometria SAR satellitare, in grado di monitorare fenomeni di deformazione con accuratezza millimetrica tramite l'osservazione di un limitato numero di punti di misura (i PS). Nonostante la tecnica PS sia uno strumento operativo già da alcuni anni, la natura fisica dei punti di misura osservati dal satellite è tutt'oggi oggetto di investigazione. La conoscenza della natura fisica dei PS è un passo fondamentale nell'interpretazione dei fenomeni di deformazione e per una corretta ricostruzione della topografia. Scopo del presente lavoro è mostrare i risultati della caratterizzazione dei PS, ottenuti utilizzando 120 immagini acquisite dai satelliti ERS ed ENVISAT della zona urbana della città di Milano.

1. INTRODUCTION

The Permanent Scatterers (PS) technique is a powerful operational tool for monitoring ground deformations on a large number of natural coherent targets (up to 300 PS/Km^2 in urban areas), exploiting long series of SAR data (Ferretti A. 2000; Ferretti A. 2001). The most attractive aspect of this approach is the capability of providing measurements relative to individual radar targets with unprecedented precision. Even if the PS technique has been used since the late nineties, the physical nature of PS's is still under investigation as a key step for a correct interpretation of the measured deformation mechanism. As an example, the phase of a dihedral formed by the ground and a building wall does not change in presence of buildings slow subsidence, but it changes in case of ground subsidence (Ketelaar V.B.H. 2003). In second instance, the classification of reflecting structures behaving as PS allows an a-priori identification of the PS's looking at the structural details of buildings. Finally, if we know the PS's physical nature, we can foresee their electromagnetic behaviour under different acquisition geometries, frequencies and polarizations, and we can develop feasibility studies on the integration of interferometric SAR multiple sensors (e.g. ERS and ENVISAT coherent exploitation (Colesanti C. 2003; Perissin D. 2004) or the future Radarsat 1 and Radarsat 2 coherent exploitation). In this paper we describe the methodology adopted to tackle the problem of the urban PS physical nature and we report the principal results we obtained.

2. PHYSICAL ANALYSIS

The present work is based on the analysis of 120 SAR images of town of Milano where ground truth data are easily accessible to us. The 120 SAR images dataset has been acquired by ERS-1, ERS-2 and ENVISAT satellites from 1992 to 2005. Normal baseline values range from -4000 to 4000 m and Doppler Centroid from -4 to 4 PRF (such a wide DC range is mainly due to ERS-2 acquisitions in gyro-less mode). Moreover, two 16MHz spectral bands centred around 5.3GHz (ERS radar frequency) and 5.331GHz (ENVISAT radar frequency) have been exploited. The processed area covers 16x18 Km^2 around the city-centre. Four different measurements have been carried out for each PS: the elevation with respect to the ground, the radiation pattern, the auto-interferogram phase of an ENVISAT alternating polarization acquisition and the phase dependence on the air temperature measured at the SAR acquisition time.

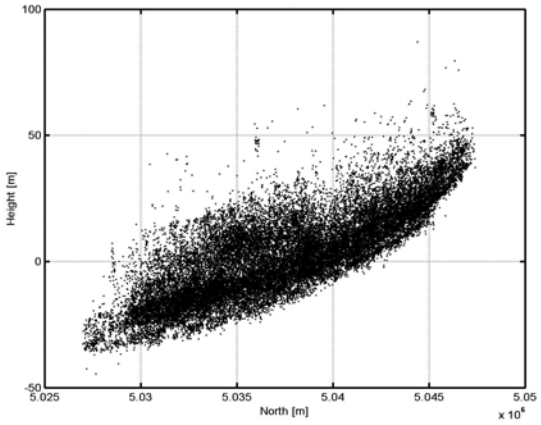

Figure 1. PS estimated elevations as a function of the North (Gauss-Boaga) coordinate in Milan. Average slope in the order of 3m per km.

2.1 Elevation

The PS location should be known within a few meters accuracy in the 3D space to be able to associate the PS to a physical structure. To this aim we exploit the PS relative height that, together with the deformation rate, is the principal product of the PS analysis. The PS approach is described in detail in (Ferretti A. 2000; Ferretti A. 2001). Here, we wish briefly recall that, for a given PS with slant range position and elevation respectively Δr and Δq (relative to the centre of the sampling cell), the following expression of the geometric component of the interferometric phase holds:

$$\Delta\phi = \frac{4\pi}{\lambda}\left(\Delta r \frac{B_n}{R_M \tan\theta} + \Delta q \frac{B_n}{R_M \sin\theta}\right) \qquad (1)$$

Here λ is the radar wavelength, B_n the Normal Baseline, R_M the sensor-target distance and θ the incidence angle. The first term is related to the flat terrain and can be compensated exploiting the WGS84 ellipsoid and the satellite state vectors. The second term contains the target height, which can be estimated as the

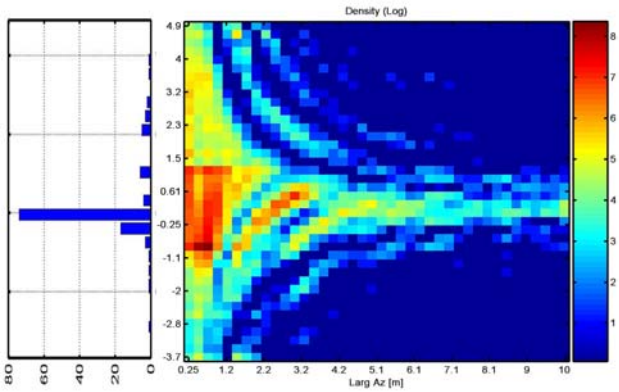

Figure 3. PS's azimuth geometric conformation (Milan dataset). Colour scale indicates the density of PS's in a log scale. Y-axis: PS's orientation as a function of normalized Doppler Centroid [Hz/PRF]. X-axis: PS's azimuth extension [m]. This extension can be larger than one cell, as the phase response has central symmetry and the amplitude one is windowed by the ground reflectivity pattern. Left: normalized Doppler Centroids histogram.

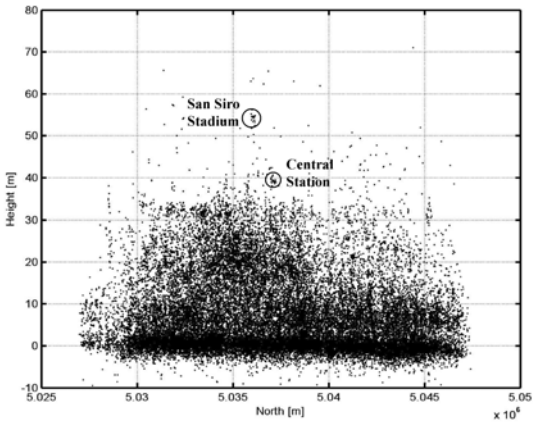

Figure 2. North-South profile of Milan city after removing for the low-pass topography. It is worth noting the thickening of high points around the centre of Milan, where the buildings are higher and closer among themselves. Focusing the attention on details, some set of adjacent points with high elevations describing high regular structures can be appreciated, e.g. the Central Station and San Siro Stadium.

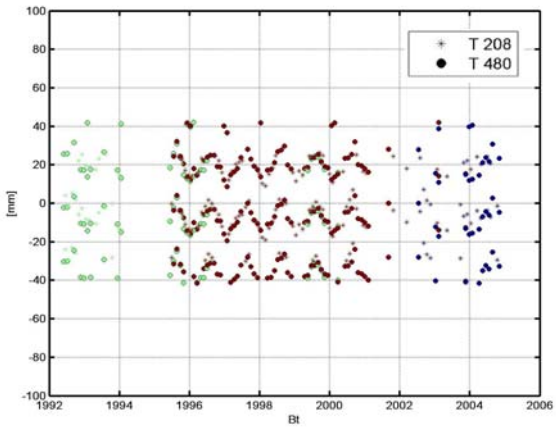

Figure 4. An example of Displacement time series [mm] measured by ERS and ENVISAT from 2 different parallel tracks 40km apart. Stars: track 208, circles: track 480. Green dots: ERS-1. Red dots: ERS-2. Blue dots: ENVISAT.

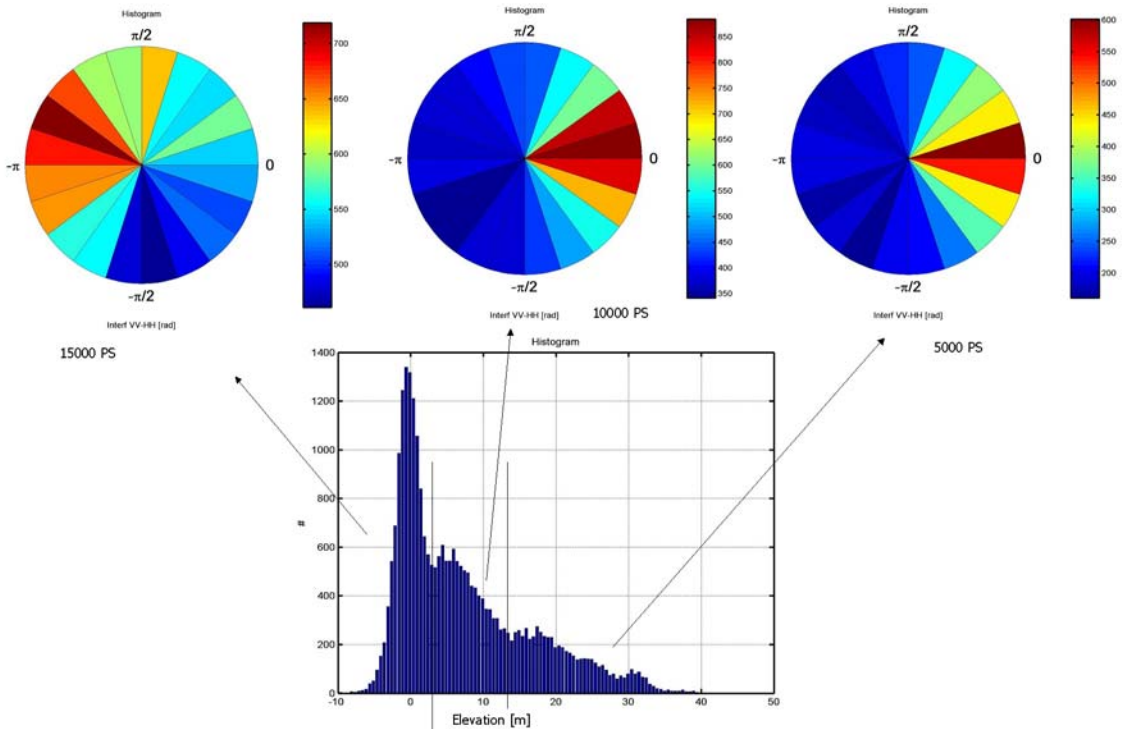

Figure 5. Alt. Pol. auto-interferogram phase [rad] histograms for different elevation classes. Below: PS's elevation [m] histogram.

value that fits the measurement. In Figure 1 we report the PS's ellipsoidal elevation so found along the North (Gauss-Boaga) coordinate. From Figure 1 the average 3m per km N-S slope of the area of Milano can be easily appreciated. The PS elevation referred to the surrounding ground level can be achieved by estimating and subtracting the lower envelope of the cloud of points in Figure 1. The result obtained is shown in Figure 2. Focusing the attention on details, one can appreciate some set of adjacent points with high elevations, describing high regular structures. It is worth noting the thickening of high points around the centre of Milan, where the buildings are higher and closer among themselves. We wish to point out that such a precision of PS height estimate is due to the high dispersion of Normal Baseline values, ranging from -4000 to 4000 m. With such a dataset, despite of the presence of a few outliers showing strong negative elevation, the achieved average elevation accuracy is close to 1m (Ferretti A. 2004).

2.2 Amplitudes analysis

The identification of each PS backscattering pattern as a function of Normal Baseline and Doppler Centroid is the second step of the PS's characterization. It should be pointed out that ERS-2 loss of gyroscopes, usually seen as a negative fact, turns out to be a very positive circumstance to get the microwave radiation pattern of each scatterer also in the azimuth direction. The PS backscattering radiation pattern has been modelled with a cardinal sine both in range and azimuth domains. Each PS is thus identified by 4 parameters: width and orientation in range and azimuth directions. As far as range is concerned, the PS backscattering radiation pattern observed by the satellite as a function of the Normal Baseline B_n is a cardinal sine whose main lobe width is inversely proportional to the target extension L_x measured along the normal to the slant range. The main lobe position B_{n0} on the Normal Baseline axis indicates the target pointing.

$$s(B_n) = \mathrm{sinc}\left[\frac{2L_x}{\lambda R_M}(B_n - B_{n0})\right] \qquad (2)$$

Likewise we obtain for the azimuth dimension a backscattering radiation pattern as a function of the Doppler centroid variation with respect to the master image Δf_{DC}:

$$s(\Delta f_{DC}) = \mathrm{sinc}\left[\frac{L_{az}}{PRF\,\delta_{az}}(\Delta f_{DC} - \Delta f_{DC0})\right] \qquad (3)$$

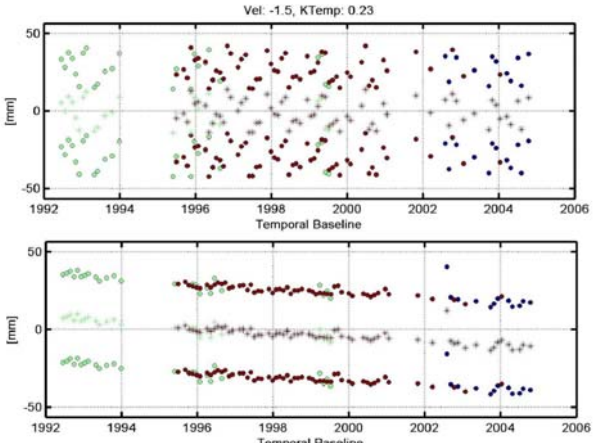

Figure 6. Displacement time series [mm] example. Green dots: ERS-1, red dots: ERS-2, blue dots: ENVISAT. Above: without removing the temperature-dependent term. Below: after removal of the temperature-dependent term. The 2 adjacent replica (± 28 mm) are plotted in order to elucidate ambiguities.

Here *PRF* is the pulse repetition frequency and δ_{az} the azimuth sampling step. It should be pointed out that modelling the backscattering radiation pattern as a cardinal sine is quite a strong hypotesis. Nonetheless it has been seen that this is the case for most of the identified PS. In Figures 3 the results of the estimated PS azimuth dimensions are shown. The colour scale of Figure 3 indicates the PS's density in Milano as a function of the estimated PS's azimuth extension (x-axis) and PS azimuth orientation (y-axis). The azimuth orientation is expressed as the normalized Doppler Centroid (Hz/PRF) deviation with respect to the master image, which is barycentric within the dataset. Figure 3 shows that large coherently observed PS's (on the right of the image) are mainly pointed toward the master acquisition since their radiation pattern is narrow. On the other hand, narrow PS's (on the left of the image) do not show such a strict pointing requirement since their radiation pattern is wider. On the same image it can be observed that some of the PS's are seen through their secondary lobes that are separated by the main lobe by an angle (vertical on the image) that is inversely proportional to the PS azimuth dimension. In between there are the zeros of the radiation pattern that generate null density areas clustering along curves clearly visible in Figure 3. It should be pointed out that PS azimuth dimensions larger than the resolution cell (about 5 meters for ERS and Envisat) can be detected.

Narrow PS's with a wide scattering pattern should remain coherent when observed from different acquisition geometries. A PS with the very same 3D location in images acquired with different looking angle is reported in Figure 4. Here, data acquired from 2 different ERS and ENVISAT parallel tracks (208 and 480) with 3° incidence angle difference are plotted together, showing very high coherence.

From a technical point of view it should be emphasized that images co-registration is much more critical when working on amplitudes than on phases of interferometric images. In the case of ERS and ENVISAT SAR data, coregistration errors as small as 50cm should be achieved to get useful information from amplitudes time series.

2.3 Alternating Polarization

In the alternating polarization acquisition mode, ENVISAT takes simultaneously 2 images with 2 different polarizations of the same area, with the same acquisition geometry but with half azimuth resolution. Creating an interferogram between the two images (auto-interferogram), in correspondence "good" scatterers (where the 2 different spectra are coherent) the interferometric phase depends only on the polarimetric response of the scatterers (Inglada J. 2004). Thus the polarimetric auto-interferogram can be exploited for discerning between odd and even bounces. A specular reflector (a mirror) behaves in the same way if illuminated with horizontal or vertical polarised signals (0 auto-interferometric phase), whereas a dihedral rotates the phase by π radians (Inglada J. 2004; Van Zyl PJ. 1989).

In Figure 5 three histograms of the auto-interferometric phase are shown for different elevation classes of the PS's in Milan. It's interesting to observe that the probability to have dihedrals at the ground level is quite high, while at higher elevations odd-bounces dominate (tiled roofs or corrugated iron roofs are good back-scatterers).

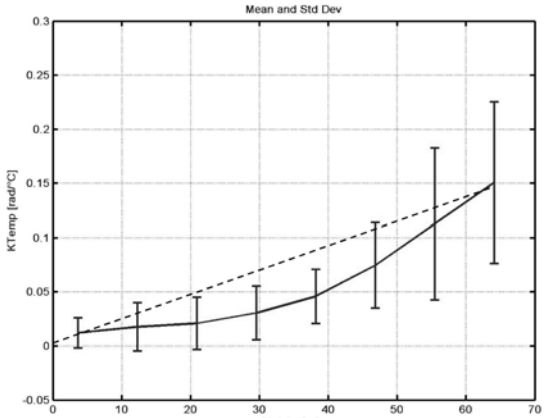

Figure 7. Mean value and dispersion (sign at ±σ) of PS's thermal dilation as a function of the estimated elevation. Dashed line: theoretic behavior of composite-steel buildings.

2.4 Temperatures

The last element taken into account is the correlation between the PS phase time series and temperatures taken at the acquisition time. This measurement does not refer to the target itself, but to the structure on which it lays. In fact, the phase oscillations are normally due to the thermal dilation of high composite steel-concrete buildings. The formula for linear expansion for a solid is

$$\Delta L = \alpha L_0 \Delta T \qquad (4)$$

PS Type:	Dihedral
Coherence:	0.95
Av. def. trend:	-1 [mm/years]
Height:	+1 [m]
K temp-phase:	+0.01 [rad/°C]
AP phase VV-HH:	-2.4 [rad]
AP ampl. dev.:	0.0
RCS:	16000 [m^2]
Fitting index:	0.91
K temp-ampl.:	+0.0e-2 [°C^-1]
Ton:	1992.5 [years]
Toff:	2004.6 [years]
Range width:	0 [m]
Azimuth width:	5 [m]
Range pointing:	+300 [m]
Azimuth pointing:	+0.0 [Hz/PRF]

Fig. 8. PS example in Milan: dihedral in a park. Left: aerial photo and PS position. Centre: target photo. Right: list of the PS estimated parameters (height h=0m, point-wise in range L_x=0m, AP phase –2.4rad).

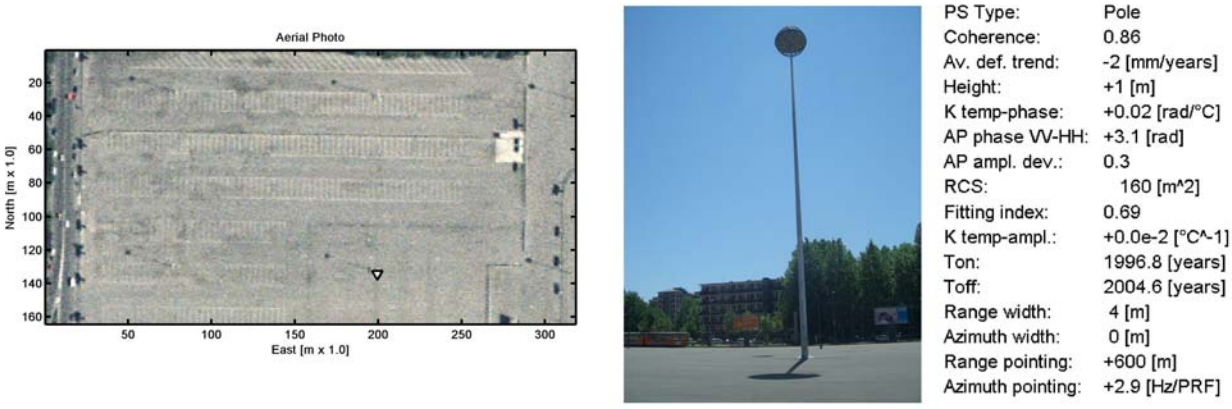

Fig. 9. PS example in Milan: pole on a car park. Left: aerial photo and PS position. Centre: target photo. Right: list of the PS estimated parameters (height h=0m, low RCS, small L_x=4m L_y=0m, AP phase 3.1rad).

A change in temperature ΔT causes a dilation of ΔL for an object of length L_0. The constant of proportionality α is called the coefficient of linear expansion and depends on the material. Assuming a thermal expansion coefficient of $1 \cdot 10^{-5}$ (composite steel concrete buildings) and a temperature range of 30°C, a 24 mm oscillation corresponds to an 80m high building. This is the case depicted in Figure 6 where an example of displacement time series before and after the subtraction of the temperature-dependent term is shown. The oscillation range is thus related to the building height, as can be seen in Figure 7. The PS's thermal dilation is plotted in correspondence of their elevation as estimated in the Milan site.

As seen, the oscillating term can affect enormously the series coherence. We couldn't find structures such that reported in Figure 6 without a systematic estimation and removal of the thermal dilation component on the whole set of the analysed points.

2.5 Target typologies

The described radar measurements can be jointly exploited to identify and characterize urban SAR PS's. Thus we discovered that the principal urban target typologies are the following:

1) Dihedrals formed by wall and ground (low elevation, narrow in range, wide in azimuth, high RCS, AP phase π), see Figure 8. This kind of targets is visible from different parallel tracks.
2) Dihedrals with circular symmetry like poles (low elevation, narrow in range, narrow in azimuth, low RCS, AP phase π), see Figure 9. These are targets that can be seen from ascending and descending passes.
3) Trihedrals corresponding to internal angles of courtyards (low elevation, narrow in range, narrow in azimuth, high RCS, AP phase 0), see Figure 10. Visible from different parallel tracks.
4) Back-scattering floor gratings -periodical ground metal structures- (low elevation, wide in range, wide in azimuth, middle RCS, AP phase 0), see Figure 12. Generally not visible under different geometries.

Back-scattering roofs -periodical elevated structures- (high elevation, wide in range, wide in azimuth, middle-low RCS, AP phase 0), see Figure 11. Generally not visible under different geometries.

3. CONCLUSIONS

The results on the PS physical nature show that:

- PS's position can be measured with an accuracy of about 1m only if large baselines and Doppler centroids are exploited.
- PS's backscattering radiation pattern and thus their dimension and pointing angle can be roughly estimated by exploiting very large baselines and Doppler centroids.
- Dihedrals can be discriminated from specular or trihedrals reflectors by exploiting AP acquisitions
- The thermal dilation is an index of the structure on which the PS's are located.

Fig. 10. PS example in Milan: trihedral in a court-yard. Left: aerial photo and PS position. Centre: target photo. Right: list of the PS estimated parameters (height h=2m, high RCS, small L_x=3m L_y=0m, AP phase –0.7rad).

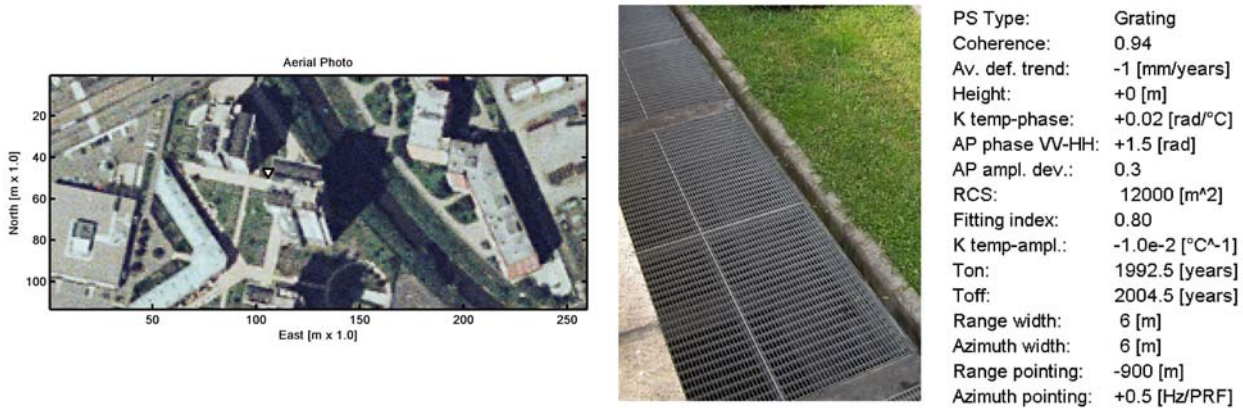

Fig. 11. PS example in Milan: floor metal grating. Left: aerial photo and PS position. Centre: target photo. Right: list of the PS estimated parameters (height h=0m, width L_x=6m L_y=6m, temperature-dependency k_T=-.01°C^{-1}).

- Urban SAR PS's typologies, recognizable by means of radar measurements, are dihedrals, poles, trihedrals, floor gratings, roofs.
- Urban SAR PS characterization allows the identifications of targets visible by different sensors.

References

Ferretti A., Prati C., Rocca F., (2001), "Permanent Scatterers in SAR Interferometry", IEEE TGARS, Vol. 39, no. 1, 2001.

Ferretti A., Prati C., Rocca F., (2000), "Non-linear subsidence rate estimation using permanent scatterers in Differential SAR Interferometry", IEEE TGARS, Vol. 38, no. 5, 2000.

Ketelaar V.B.H., Hanssen R.F., (2003), "Separation of different deformation regimes using PS-INSAR data", Proceedings of FRINGE 2003, Frascati (Italy), 1-5 December 2003.

Colesanti C., Ferretti A., Perissin D., Prati C., Rocca F., (2003), "ERS-ENVISAT permanent scatterers interferometry", Proceedings of Geoscience and Remote Sensing Symposium, IGARSS '03. 2003 IEEE International, Volume: 2, Pages: 1130 - 1132 vol.2.

Ferretti A., Perissin D., Prati C., Rocca F., (2004), "ERS-ENVISAT Permanent Scatterers", Proceedings of Geoscience and Remote Sensing Symposium IGARSS 2004, Anchorage (Alaska), September 2004.

Ferretti A., Prati C., Rocca F., (2004), "Requirements for a space mission for DInSAR and PS analysis based on past and present missions", Proceedings of IGARSS '04. 2004 IEEE International Volume 3, Page(s): 1695 - 1698 vol.3

Inglada J., Henry C., Souyris J-C., (2004), "Assessment of ASAR/IMS Multi-polarization Images Phase Difference in the Framework of Persistent Scatterers Interferometry", ENVISAT congress, Salzburg (Austria) 20-24 September 2004.

Van Zyl PJ., (1989), "Unsupervised Classification of Scattering Behaviour using RADAR Polarimetry data", IEEE Transactions on GRS, January 1989, pp 36-45.

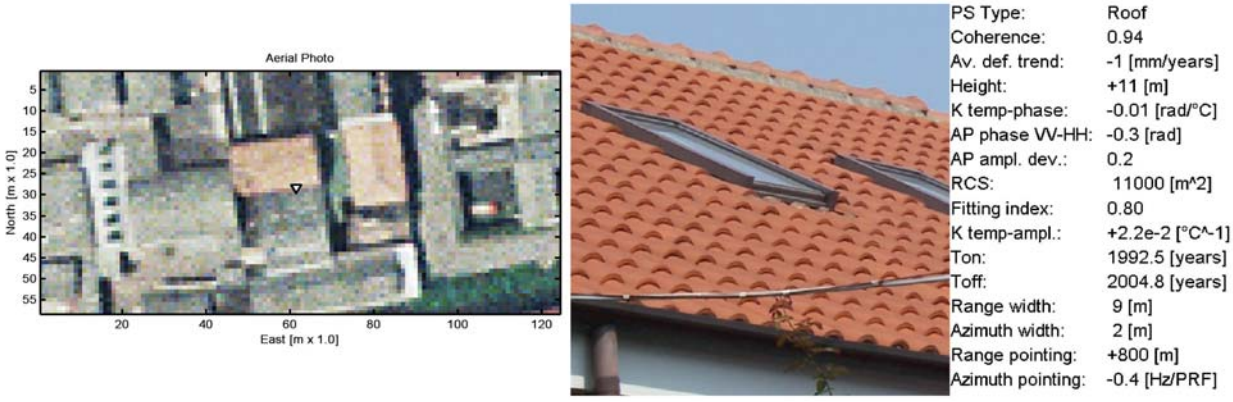

Fig. 12. PS example in Milan: tiled roof. Left: aerial photo and PS position. Centre: target photo. Right: list of the PS estimated parameters (height h=11m, width L_x=9m L_y=2m, temperature-dependency k_T=-.02°C^{-1}).